Supplementary Information

Single atom coordination in a manganese-cobalt bi-metallic framework on graphene: geometric and electronic structures

Stefania Baronio,[a] Michela De Col,[a] Asha Yadav,[b] Basant Roondhe,[b] Valentin Mischke,[c] Olga Resel,[d] Davide Bidoggia,[a] Alessandro Namar,[a] Nikolay Vinogradov,[e] Mattia Scardamaglia,[e] Manuel Valvidares,[f] Pierluigi Gargiani,[f] Mirko Cinchetti,[c] Giovanni Zamborlini,[c,d] Paolo Giannozzi,[b,g,*] Erik Vesselli[a,h,i,*]

[a] Department of Physics University of Trieste via A. Valerio 2, Trieste 34127, Italy

[b] Department of Mathematics, Computer Science, and Physics, University of Udine, Udine, I-33100, Italy

[c] Department of Physics, TU Dortmund University, Dortmund, 44227, Germany

[d] Institute of Physics, NAWI Graz, University of Graz, Universitätsplatz 5, 8010 Graz, Austria

[e] MAX IV Laboratory, Lund University, Lund, 22100, Sweden

[f] ALBA Synchrotron Light Source, 08290 Barcelona, Spain

[g] CNR – Istituto Officina dei Materiali, SISSA, Trieste 34136, Italy

[h] CNR – Istituto Officina dei Materiali (IOM) S.S. 14 km 163.5, Area Science Park, Basovizza, Trieste 34149, Italy

[i] Center for Energy, Environment and Transport Giacomo Ciamician, University of Trieste, Trieste 34127, Italy

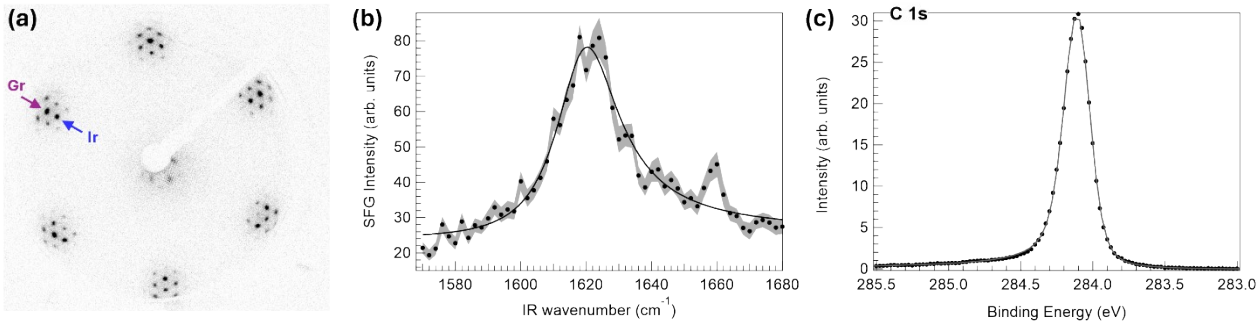

Figure S1. (a) LEED of Gr/Ir(111) at 75 eV, the arrows indicate Ir and Gr first order diffraction spots, the other are related to the moiré pattern; (b) SFG spectrum of graphene showing the G-band at 1619 cm^{-1}; (c) XPS C 1*s* core level spectrum of graphene on Ir(111) - photon energy 400 eV.

The LEED pattern (Figure S1a), collected at an electron kinetic energy of 75 eV, shows graphene grown at 1275 K, where the spots relative to the Ir surface and graphene are indicated by the arrows, and the coincidence lattice contribution induced by the moiré is visible as sharp spots surrounding them.[1–4] The good quality of the graphene layer is demonstrated by the visibility of higher diffraction order spots and the moiré spots,[2,3] and the absence of arches, associated with rotational domains.[5] The Ir-Vis SFG graphene spectrum (Figure S1b) shows the G-phonon resonance,[6–8] observed at 1619 cm^{-1}, with Γ = 12 cm^{-1}, which is related to the in-plane sp^2 C-C stretching mode.[7,9] The graphene C 1*s* spectrum measured with a photon energy of 400 eV (Figure S1c) is well reproduced by a single sharp peak at 284.1 eV, in agreement with the literature.[4,10]

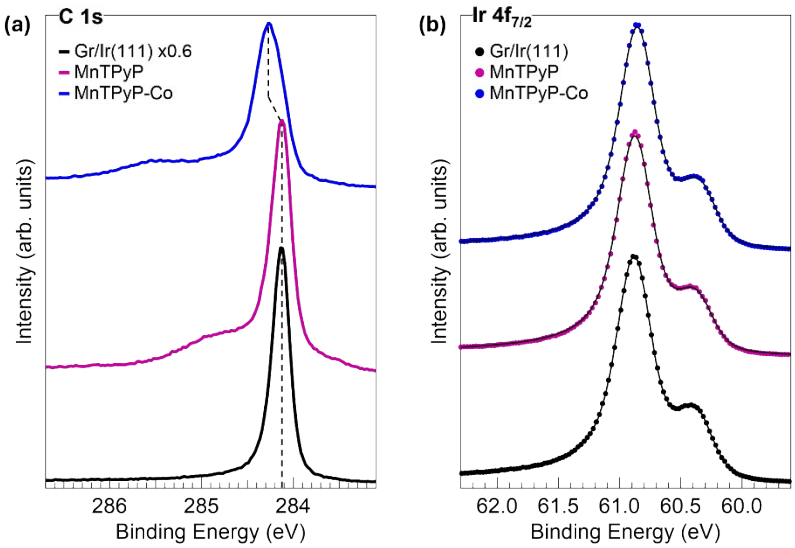

Figure S2. (a) C 1s and (b) Ir 4 $f_{7/2}$ of bare graphene, 1 ML MnTPyP and 1 ML MnTPyP-Co. (a) The monolayer spectrum shows a screened graphene peak and a shoulder at higher binding energy, associated to the porphyrins. Co coordination induces a shift of +0.18 meV of the graphene peak and +0.5 eV of the molecular carbon shoulder. (b) Ir 4 $f_{7/2}$ data are shown together with the best fit (black lines) that reveal the absence of chemical shift of the surface component, which shows a slight intensity modulation between different systems. The Ir $4f_{7/2}$ spectrum of Gr/Ir(111) in Figure S2 shows the bulk peak at 60.9 eV[11] and the surface peak, with a -0.52 eV surface core level shift, in agreement with previous works.[4]

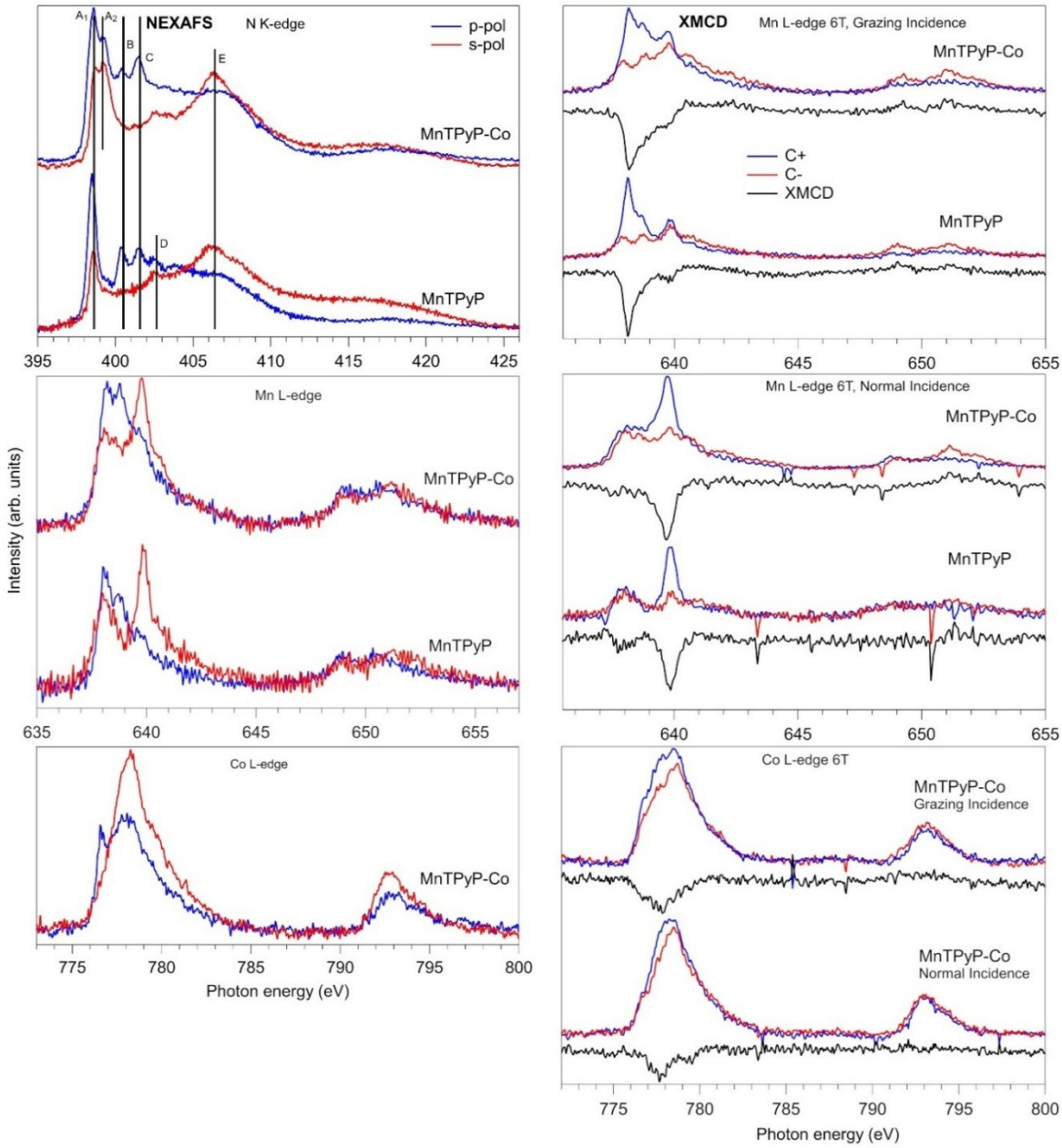

Peak	Energy (eV)	Assignment	Literature (eV)
A_1	398.5-398.6	macrocycle	398.35-398.7[12,13]
		pyridyl	398.8[14]
A_2	399.2	pyridyl	399.04-399.29[15]
B	400.4	macrocycle	400.6-401.0[12,13]
C	401.5	macrocycle	401.45-401.9[12,13]
D	402.5	pyridyl	402.6[14]
E	406.3	macrocycle	405.6-406.7[13]

Figure S3. NEXAFS (left) and XMCD (right) spectra of the MnTPyP and MnTPyP-Co layers. Labels in the NEXAFS N edge panel correspond to the assignments noted in the table here above.

Mn(II)			
MnTPyP(this work)	**MnO**[16–18]	**MnTPP**[19]	**MnPc**[20]
640.5	640.0-640.3	640.1	640.5
	641.1-641.2	640.9	
641.9	642.0-642.1	641.9	642.5
643.4	642.9-644.2	643.1	
646.9	645-646.2	644.4	645.5
Mn(III)			
MnTPyP-Co(this work)	**MnOOH**[16–18]	**MnO_2**[16]	
641.0	640.7-641	640.7	
	641.4-641.9	641.4	
642.3	642.2-642.5	642.2	
	643-643.5	643.2	
643.8	643.8-644.9	644.6	
647.2	645.7-646.2		

Table S1. Mn $2p_{3/2}$ experimental binding energies (eV) of Mn(II) and Mn(III) composites (manganese oxide, dechlorinated MnTPP/Ag(111), MnPc, manganite, birnessite) compared to the results of this work (reported in the first column). Based on the literature data, we conclude that MnTPyPs contain Mn(II) in the mono-metallic layer and a Mn(II)-Mn(III) intermediate configuration in the bi-metallic framework.

N species	**MnTPyP**(this work)	**FeTPyP**[15]	**CoTPyP**[15]	**2HTPyP**[21]	**MnPc**[20,22,23]
Iminic	397.8	398.5	398.8	397.4	398.5-398.6
Pyridinic	398.3	398.9	399.1	398.3	
ΔE	0.50	0.46	0.28	0.9	
Shake-up	399.3	400.0	400.3		
N species	**MnTPyP-Co**(this work)	$\Delta E'$	**FeTPyP-Fe**[15]	$\Delta E'$	**CoTPyP-Fe**[15]	$\Delta E'$
Iminic	398.7	+0.9	399	+0.47	399.0	+0.21
Pyridinic	400.0	+1.8	399.5	+0.55	399.4	+0.33
ΔE	1.34		0.54		0.42	
Shake-up	401.4					

Table S2. N 1*s* experimental binding energies and energy shifts from this work, compared with the corresponding species in FeTPyP and CoTPyP/Gr/Ir(111). All values are in eV. ΔE is the energy difference between the iminic and pyridinic components. The bimetallic layers are compared in the bottom row of the table, ΔE' refers to the relative chemical shift induced by the coordination of a second metal atom.

	Co(I)	Co(I)-Co(II)	Co(II)	Co(II)	Co(0)
MnTPyP-Co(this work)	**CoTPyP-Co**[15]	**CoTPP**[24–26]	**CoTPYP**[15]	**CoO**[17]	**Co**[17,27]
778.5*	778.6	778.2*	779.4*		778.1
780.0		780	780.1	780	781.1
781.6			782.1	782.1	783.1
784.7			784.3	785.5	
				786.5	

Table S3. Co $2p_{3/2}$ experimental binding energies from this work, compared with known reference Co oxidation states - Co(0), Co(I) and Co(II) - from the literature. According to our assignments, when tetracoordinated with the pyridyl moieties of the MnTPyPs, Co is in oxidation state +1, as in the case of CoTPyP-Co/Gr and CoTPP/Ag(111) or Cu(100). The (*) indicates a Gunnarsson-Schönhammer (GS) feature, as explained in the text. Reporting literature information, we find that Co in CoTPP lead to ambiguous assignments, with a +2 oxidation state both for mono- and multi-layers on CuO, and in reduced form at the interface with: thus, the low binding energy component can be assigned both to the effective reduction to Co(I) as well as to a GS feature.

	Spin	d_{z^2}	d_{xz}	d_{yz}	$d_{x^2-y^2}$	d_{xy}
MnTPyP/Gr (single molecule)						
Mn	up	**0.961**	**0.985**	**0.994**	**0.995**	**0.997**
	down	0.026	0.040	0.044	0.054	0.308
MnTPyP/Gr						
Mn1	up	**0.956**	**0.985**	**0.995**	**0.995**	**0.997**
	down	0.027	0.040	0.046	0.053	0.311
Mn2	up	0.630	**0.984**	**0.990**	**0.994**	**0.996**
	down	0.039	0.063	0.064	0.428	0.487
MnTPyP-Co/Gr (Co saturation)						
Mn1	up	0.467	**0.975**	**0.982**	**0.983**	**0.989**
	down	0.047	0.053	0.058	0.339	**0.976**
Mn2	up	0.467	**0.975**	**0.982**	**0.983**	**0.989**
	down	0.047	0.053	0.058	0.339	**0.976**
Co1	up	**0.987**	**0.990**	**0.994**	**0.996**	**0.996**
	down	0.024	0.137	**0.977**	**0.986**	**0.990**
Co2	up	**0.987**	**0.990**	**0.994**	**0.995**	**0.996**
	down	0.024	0.138	**0.977**	**0.986**	**0.990**
MnTPyP-Co/Gr (half Co saturation)						
Mn1	up	0.892	**0.985**	**0.993**	**0.993**	**0.996**
	down	0.034	0.054	0.062	0.078	0.367
Mn2	up	0.893	**0.985**	**0.993**	**0.993**	**0.996**
	down	0.034	0.054	0.062	0.076	0.367
Co	up	0.024	0.139	**0.975**	**0.985**	**0.989**
	down	**0.988**	**0.990**	**0.994**	**0.995**	**0.996**

Table S4. Spin-resolved, actual occupation of the *d*-orbitals resulting from the DFT calculations for (from top to bottom of the table): the single MnTPyP molecule in graphene, a full MnTPyP monolayer, the MnTPyP-Co layer at full and half saturation. Mn1, Mn2, Co1 and Co2 labels refer to the two slightly non-equivalent Co and Mn atoms in the unit cell due to the different matching with the underlying graphene sheet.

MnTPyP	MnTPyP-Co	Mode Assignment
1222		
	1225	δ(pyr)
1243		
	1257	$\nu(C_\alpha{-}N) + \delta(C_\beta{-}H)$, $\nu(C_m{-}pur) + \delta(C{-}H)_{pyr}$
1339		
	1348	
1351		$\nu(C_\alpha{-}N)$
	1367	
	1419	
	1439	$\nu(C_\alpha{-}N) + \delta(C_\beta{-}H)$, $\nu(C_\alpha{-}C_\beta)$
1496		
	1497	$\nu(C_\alpha{-}C_\beta)$, $\nu(C_\beta{-}C_\beta)$
1522		δ(pyr)
1538		$\nu(C_\beta\text{-}C_\beta)+\delta(C_\beta\text{-}H)$, $\nu(C_\beta\text{-}C_\beta)$, $\nu(C_\beta\text{-}H)$
	1539	δ(pyr)
	1546	$\nu(C_\beta\text{-}C_\beta)+\delta(C_\beta\text{-}H)$, $\nu(C_\beta\text{-}C_\beta)$, $\nu(C_\beta\text{-}H)$
1559		$\nu(C_\alpha{-}C_m)$, $\nu(C_m{-}C_m)$
	1595	
1599		δ(pyr), $\nu(C\text{-}C)_{pyr}$
	1617	δ(pyr)
1618		Graphene G-mode
2984		
3023		
	3031	
	3063	$\nu(C_\alpha{-}H)$
3067		
	3090	

Table S5. IR-Vis SFG vibrational resonances positions for the MnTPyP and MnTPyP-Co MOFs on Gr/Ir(111), in cm^{-1}. Mode attribution by comparison with experimental values for FeTPyP,[28,29] CoTPyP,[30,31] ZnTPyP,[32] 2HTPyP,[33] MnTPPCl,[34] and graphene.[6–8] The vibrational modes notation is the standard used in the literature.[28,29,33]

References.

1 A. T. N'Diaye, J. Coraux, T. N. Plasa, C. Busse and T. Michely, *New J. Phys.*, DOI:10.1088/1367-2630/10/4/043033.
2 M. Endlich, H. P. C. Miranda, A. Molina-Sánchez, L. Wirtz and J. Kröger, *Ann. Phys.*, 2014, **526**, 372–380.
3 I. Pletikosić, M. Kralj, P. Pervan, R. Brako, J. Coraux, A. T. N'Diaye, C. Busse and T. Michely, *Phys. Rev. Lett.*, 2009, **102**, 056808.
4 P. Lacovig, M. Pozzo, D. Alfè, P. Vilmercati, A. Baraldi and S. Lizzit, *Phys. Rev. Lett.*, 2009, **103**, 166101.
5 H. Hattab, A. T. N'Diaye, D. Wall, G. Jnawali, J. Coraux, C. Busse, R. van Gastel, B. Poelsema, T. Michely, F.-J. M. zu Heringdorf and M. H. Hoegen, *Appl. Phys. Lett.*, DOI:10.1063/1.3548546.
6 A. A. Taleb, G. Anemone, D. Farías and R. Miranda, *Carbon*, 2018, **133**, 31–38.
7 R. Beams, L. G. Cançado and L. Novotny, *J. Phys. Condens. Matter*, 2015, **27**, 083002.
8 M. Corva, F. Mohamed, E. Tomsic, M. Rinaldi, C. Cepek, N. Seriani, M. Peressi and E. Vesselli, *J. Phys. Chem. C*, 2019, **123**, 3916–3922.
9 F. Tuinstra and J. L. Koenig, *J. Chem. Phys.*, 1970, **53**, 1126–1130.
10 C. Botta, F. Loi, D. Alfè and A. Baraldi, *Appl. Surf. Sci.*, 2024, **646**, 158913.
11 M. Bianchi, D. Cassese, A. Cavallin, R. Comin, F. Orlando, L. Postregna, E. Golfetto, S. Lizzit and A. Baraldi, *New J. Phys.*, 2009, **11**, 063002.
12 M. P. De Jong, R. Friedlein, S. L. Sorensen, G. Ãhrwall, W. Osikowicz, C. Tengsted, S. K. M. Jönsson, M. Fahlman and W. R. Salaneck, *Phys. Rev. B - Condens. Matter Mater. Phys.*, 2005, **72**, 1–8.
13 N. Schmidt, R. Fink and W. Hieringer, *J. Chem. Phys.*, DOI:10.1063/1.3435349.
14 C. Kolczewski, R. Püttner, O. Plashkevych, H. Ågren, V. Staemmler, M. Martins, G. Snell, A. S. Schlachter, M. Sant'Anna, G. Kaindl and L. G. M. Pettersson, *J. Chem. Phys.*, 2001, **115**, 6426–6437.
15 F. Armillotta, D. Bidoggia, P. Biasin, A. Annese, A. Cossaro, A. Verdini, L. Floreano, M. Peressi and E. Vesselli, *Cell Rep. Phys. Sci.*, 2023, **4**, 101378.
16 H. W. Nesbitt and D. Banerjee, *Am. Mineral.*, 1998, **83**, 305–315.
17 M. C. Biesinger, B. P. Payne, A. P. Grosvenor, L. W. M. Lau, A. R. Gerson and R. S. C. Smart, *Appl. Surf. Sci.*, 2011, **257**, 2717–2730.
18 E. S. Ilton, J. E. Post, P. J. Heaney, F. T. Ling and S. N. Kerisit, *Appl. Surf. Sci.*, 2016, **366**, 475–485.
19 J. P. Beggan, S. A. Krasnikov, N. N. Sergeeva, M. O. Senge and A. A. Cafolla, *Nanotechnology*, DOI:10.1088/0957-4484/23/23/235606.
20 J. L. Zhang, Z. Wang, J. Q. Zhong, K. D. Yuan, Q. Shen, L. L. Xu, T. C. Niu, C. D. Gu, C. A. Wright, A. Tadich, D. Qi, H. X. Li, K. Wu, G. Q. Xu, Z. Li and W. Chen, *Nano Lett.*, 2015, **15**, 3181–3188.
21 Y. Li, J. Xiao, T. E. Shubina, M. Chen, Z. Shi, M. Schmid, H. P. Steinrück, J. M. Gottfried and N. Lin, *J. Am. Chem. Soc.*, 2012, **134**, 6401–6408.
22 F. Haidu, O. D. Gordan, D. R. T. Zahn, L. Smykalla, M. Hietschold, B. V. Senkovskiy, B. Mahns and M. Knupfer, *arXiv*, DOI:doi.org/10.48550/arXiv.1702.03575.
23 M. Panighel, PhD Thesis, University of Trieste, 2015.
24 W. Hieringer, K. Flechtner, A. Kretschmann, K. Seufert, W. Auwärter, J. V. Barth, A. Görling, H. P. Steinrück and J. M. Gottfried, *J. Am. Chem. Soc.*, 2011, **133**, 6206–6222.
25 I. Cojocariu, S. Carlotto, G. Zamborlini, M. Jugovac, L. Schio, L. Floreano, M. Casarin, V. Feyer and C. M. Schneider, *J. Mater. Chem. C*, 2021, **9**, 12559–12565.
26 T. Lukasczyk, K. Flechtner, L. R. Merte, N. Jux, F. Maier, J. M. Gottfried and H.-P. Steinrück, *J. Phys. Chem. C*, 2007, **111**, 3090–3098.
27 A. A. Khassin, T. M. Yurieva, V. V. Kaichev, V. I. Bukhtiyarov, A. A. Budneva, E. A. Paukshtis and V. N. Parmon, *J. Mol. Catal. Chem.*, 2001, **175**, 189–204.
28 S. Popovici, W. Leyffer and R. Holze, *J. Porphyr. Phthalocyanines*, 1998, **2**, 249–260.
29 N. Blom, J. Odo, K. Nakamoto and D. P. Strommen, *J. Phys. Chem.*, 1986, **90**, 2847–2852.
30 F. Armillotta, D. Bidoggia, S. Baronio, A. Sala, R. Costantini, M. dell'Angela, I. Cojocariu, V. Feyer, A. Morgante, M. Peressi and E. Vesselli, *Adv. Funct. Mater.*, 2024, **34**, 2408200.
31 F. Armillotta, A. Pividori, M. Stredansky, N. Seriani and E. Vesselli, *Top. Catal.*, 2020, **63**, 1585–1595.
32 K. Araki, P. S. Santos, L. F. C. C. de Oliveira and H. E. Toma, *Spectrosc. Lett.*, 1995, **28**, 119–126.

33 J. R. T. Dos Reis, F. F. Leite, K. Sharma, G. A. S. Ribeiro, W. H. N. Silva, A. A. Batista, A. R. Paschoal, W. Paraguassu, M. Mazzoni, N. M. Barbosa Neto and P. T. Araujo, *Molecules*, 2024, **29**, 2362.
34 S. R. Alharbi, A. A. A. Darwish, S. E. Al Garni, H. I. ElSaeedy and K. F. Abd El-Rahman, *Infrared Phys. Technol.*, 2016, **78**, 77–83.